# Influence of single-neutron stripping on near-barrier $^6$He $+^{208}$Pb and $^8$He $+^{208}$Pb elastic scattering

G. Marquínez-Durán,[1] N. Keeley,[2,*] K. W. Kemper,[3] R. S. Mackintosh,[4] I. Martel,[1] K. Rusek,[5] and A. M. Sánchez-Benítez[1]

[1]*Departamento de Ciencias Integradas, Facultad de Ciencias Experimentales, Campus de El Carmen, Universidad de Huelva,*
*21071 Huelva, Spain*
[2]*National Centre for Nuclear Research, ulica Andrzeja Sołtana 7, 05-400 Otwock, Poland*
[3]*Department of Physics, Florida State University, Tallahassee, Florida 32306, USA*
[4]*School of Physical Sciences, The Open University, Milton Keynes MK7 6AA, United Kingdom*
[5]*Heavy Ion Laboratory, University of Warsaw, Warsaw, Poland*

The influence of single-neutron stripping on the near-barrier elastic scattering angular distributions for the $^{6,8}$He $+^{208}$Pb systems is investigated through coupled reaction channels (CRC) calculations fitting recently published data to explore the differences in the absorptive potential found in the scattering of these two neutron-rich nuclei. The inclusion of the coupling reduces the elastic cross section in the Coulomb-nuclear interference region for $^8$He scattering, whereas for $^6$He its major impact is on the large-angle elastic scattering. The real and imaginary dynamic polarization potentials are obtained by inverting the CRC elastic scattering $S$-matrix elements. These show that the main absorptive features occur between 11 and 12 fm for both projectiles, while the attractive features are separated by about 1 fm, with their main structures occurring at 10.5 fm for $^6$He and 11.5 fm for $^8$He.

## I. INTRODUCTION

New precise data for the elastic scattering of $^8$He from a $^{208}$Pb target at an incident energy of 22 MeV were recently published and compared with existing data for the $^6$He $+^{208}$Pb elastic scattering at the same energy [1]. Important differences are observed in the elastic scattering angular distributions of the two isotopes: while the imaginary part of the optical model potential has a longer range for $^6$He than for $^8$He, the overall absorption, as evidenced by the total reaction cross section, is greater for $^8$He. These properties are consistent with a greater importance of breakup for $^6$He and of transfer—single-neutron stripping in particular—for $^8$He.

The larger total reaction cross section for $^8$He compared to $^6$He [1], despite the lower breakup threshold for $^6$He, suggests that other reaction channels are important. The influence on the elastic scattering of coupling to the single-neutron-stripping reaction may be calculated using the coupled reaction channels (CRC) formalism. In this work we perform CRC calculations for the $^{208}$Pb($^8$He ,$^7$He)$^{209}$Pb and $^{208}$Pb($^6$He ,$^5$He)$^{209}$Pb reactions at 22 MeV and compare their influence on the respective elastic scattering angular distributions. We further compare the dynamic polarization potentials (DPP) induced by these couplings to elucidate the observed differences in the elastic scattering of these two heavy helium isotopes.

## II. THE CRC CALCULATIONS

All CRC calculations were performed using the code FRESCO [2]. As noted in Ref. [1] and as is usual for heavy-ion elastic scattering dominated by strong absorption, the values of the individual parameters of the standard empirical optical model potentials fitting the $^6$He and $^8$He $+^{208}$Pb elastic

scattering data at 22 MeV are not well determined (although the tail of the imaginary part is well determined on a point-by-point basis). Initial elastic channel optical model (OM) potentials for both the $^8$He and $^6$He $+^{208}$Pb systems were of Woods-Saxon form, obtained by refitting the elastic scattering data of Ref. [1]; why this was done is explained later when the CRC elastic scattering $S$-matrix elements are discussed. The resulting OM parameters are given in Table I. New values of these parameters were then determined in CRC calculations using SFRESCO, the searching version of the FRESCO code, to recover the fit to the elastic scattering angular distributions when single-neutron-stripping coupling was included. This was required to avoid "double counting" because part of the empirical optical model potentials was now generated by the explicitly included stripping couplings. The resulting new OM parameters are given in Table II, together with the $\chi^2$/N values for the no-coupling and full CRC calculations. We refer to the elastic channel potentials for the CRC cases in Table II as the "bare" potentials, and these are important for determining the DPPs. The quantity $\chi^2_{\mathrm{bare}}$/N given in Table II refers to the goodness of fit with the bare potential when the coupling of the stripping channels to the elastic channel is omitted. The $^8$He and $^6$He $+^{208}$Pb parameters of Table I were used unaltered for the $^7$He $+^{209}$Pb and $^5$He $+^{209}$Pb exit channel potentials, respectively.

The $\langle ^{209}$Pb $|$ $^{208}$Pb $+ n\rangle$ overlap functions were taken from Ref. [3]. Transfers to the 0.0 MeV $9/2^+$, 0.78 MeV $11/2^+$, 1.42 MeV $15/2^-$, 1.57 MeV $5/2^+$, 2.03 MeV $1/2^+$, 2.49 MeV $7/2^+$ and 2.54 MeV $3/2^+$ states in $^{209}$Pb were included. The $\langle ^8$He $|$ $^7$He $+ n\rangle$ and $\langle ^6$He $|$ $^5$He $+ n\rangle$ overlap functions were taken from Refs. [4] and [5], respectively.

The CRC calculations are compared with the elastic scattering data in Fig. 1. The solid curves denote the results of the full CRC calculations and the dashed curves the bare, no-coupling calculations. A comparison of Tables I and II

---
*nicholas.keeley@ncbj.gov.pl

TABLE I. Optical potential parameters obtained by refitting the 22 MeV $^8$He and $^6$He $+^{208}$Pb elastic scattering data of Ref. [1]. Radii follow the convention $R_i = r_i \times A_t^{1/3}$ fm and $r_C = 1.3$ fm. These parameters were also used for the exit channel $^7$He $+^{209}$Pb and $^5$He $+^{209}$Pb optical potentials, respectively.

| Projectile | $V$ | $r_V$ | $a_V$ | $W$ | $r_W$ | $a_W$ | $\sigma_R$ (mb) | $\chi^2$/N |
|---|---|---|---|---|---|---|---|---|
| $^8$He | 143.7 | 1.631 | 0.587 | 37.1 | 1.481 | 1.148 | 1529 | 3.77 |
| $^6$He | 147.4 | 1.237 | 0.618 | 19.8 | 1.090 | 1.766 | 1425 | 0.97 |

shows that good fits to the data could be recovered simply by reducing the depth of the imaginary part of the entrance channel potential ($W$) in both cases. Thus, at this energy, coupling to the single-neutron stripping accounts for about 37% and 21% of the imaginary potentials in the $^8$He $+^{208}$Pb and $^6$He $+^{208}$Pb systems, respectively. Figure 1 shows that this is reflected in the relatively large coupling effect on the elastic scattering. If we take the reduction in $\chi^2$/N induced by the coupling, i.e., the ratio of $\chi^2_{\text{bare}}$/N to $\chi^2_{\text{CRC}}$/N, as a crude quantitative estimate of the coupling effect we find that it is stronger for $^8$He (a factor of about 3.7) than for $^6$He (a factor of about 2.9). There is also a conspicuous qualitative difference in the observed coupling effect for the two systems in that, for $^8$He $+^{208}$Pb, coupling to the single-neutron stripping gives rise to a significant reduction of the elastic scattering cross section in the region where the Coulomb-nuclear interference peak would normally occur. For $^6$He $+^{208}$Pb the single-neutron-stripping coupling effect is negligible in the same angular region.

In Table III we give the total reaction cross sections ($\sigma_R$) for the bare and CRC calculations and the summed $1n$-stripping cross sections ($\sigma_{1n}$) for the CRC calculations. The $^6$He $\sigma_{1n}$ value is similar to the result (153 mb) of a distorted-wave Born approximation calculation for the $^6$He $+^{206}$Pb system at an incident energy of 18 MeV [6], taking into account the higher incident energy here. The $^6$He $+^{206}$Pb value, as part of a wider analysis, is compatible with the measured inclusive $^4$He yield in that case. There are two things to note from this comparison: First, the much larger—by a factor of 1.8—spectroscopic factor for $^8$He $\rightarrow$ $^7$He $+ n$ compared to that for $^6$He $\rightarrow$ $^5$He $+ n$ does not give rise to a correspondingly greater summed $1n$-stripping cross section. The calculated $1n$-stripping cross sections are therefore not correlated with the influence of coupling to these channels on the entrance channel imaginary potentials as quantified by the reduction in the well depths. Second, the CRC summed $1n$-stripping cross sections are some 20% greater than the increases in the respective total reaction cross sections induced by the
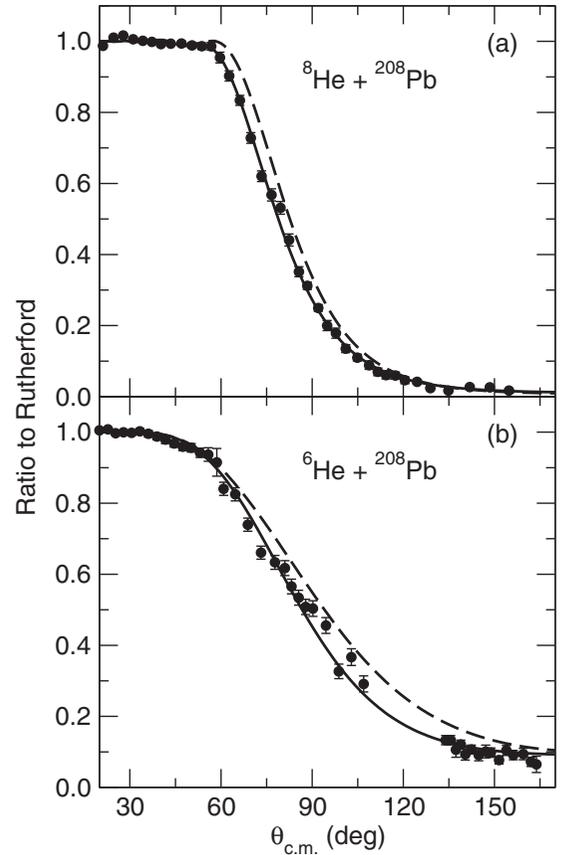


FIG. 1. (a) 22 MeV $^8$He $+^{208}$Pb elastic scattering angular distribution. (b) 22 MeV $^6$He $+^{208}$Pb elastic scattering angular distribution. The solid and dashed curves denote the full CRC and "bare", no-coupling calculations, respectively. Note the linear cross section scales.

coupling (cf. $\Delta\sigma_R = \sigma_R^{\text{CRC}} - \sigma_R^{\text{bare}}$); therefore the couplings must induce a corresponding decrease in the cross sections in other channels not considered explicitly here, e.g., fusion. This is by no means universal behavior, and channel coupling can sometimes act as a "doorway" leading to an increase in cross sections to other channels. As an example, for 30.3 MeV protons on $^{40}$Ca, coupling to neutron pickup states [7] leads to an increase in the reaction cross section about 5 times greater than the summed cross section to the states of $^{39}$Ca explicitly coupled to. However, also for 30.3 MeV protons on $^{40}$Ca, for coupling to a set of vibrational states [8], the reaction cross section increases about 24% more than the combined inelastic cross section. The other extreme occurs when channel coupling

TABLE II. Best-fit entrance-channel optical potential parameters obtained from the 22 MeV $^{208}$Pb($^8$He,$^7$He)$^{209}$Pb and $^{208}$Pb($^6$He,$^5$He)$^{209}$Pb CRC calculations. Radii follow the convention $R_i = r_i \times A_t^{1/3}$ fm and $r_C = 1.3$ fm. Values of $\chi^2$/N for these potentials are given for the no-coupling (bare, see text) and full CRC calculations.

| Projectile | $V$ | $r_V$ | $a_V$ | $W$ | $r_W$ | $a_W$ | $\sigma_R$ (mb) | $\chi^2_{\text{bare}}$/N | $\chi^2_{\text{CRC}}$/N |
|---|---|---|---|---|---|---|---|---|---|
| $^8$He | 143.7 | 1.631 | 0.587 | 23.5 | 1.481 | 1.148 | 1525 | 14.4 | 3.93 |
| $^6$He | 147.4 | 1.237 | 0.618 | 15.6 | 1.090 | 1.766 | 1412 | 4.69 | 1.61 |

TABLE III. Total reaction cross sections ($\sigma_R$) for the bare and CRC calculations and summed $1n$-stripping cross sections ($\sigma_{1n}$) for the CRC calculations. See text for an explanation of $\Delta\sigma_R$.

| Projectile | $\sigma_R^{\text{bare}}$ (mb) | $\sigma_R^{\text{CRC}}$ (mb) | $\Delta\sigma_R$ (mb) | $\sigma_{1n}$ (mb) |
|---|---|---|---|---|
| $^8$He | 1321 | 1525 | 204 | 243 |
| $^6$He | 1229 | 1412 | 183 | 219 |

leads to a *decrease* in total reaction cross section, as is the case for $^6$Li breakup in Ref. [9].

Given that the $1n$-stripping reaction is similarly well matched in $Q$ value and angular momentum for the two cases it may seem surprising that the calculated stripping cross sections ($\sigma_{1n}$) do not differ by approximately the same factor (1.8) as the projectile overlap spectroscopic factors, the target overlap spectroscopic factors being the same. However, the exit channel optical potentials are different in the two cases and test calculations employing identical parameters (the $^6$Li global potential of Cook [10]) for each system found that while the elastic scattering was almost unaffected the predicted stripping cross sections did change significantly. The $^{208}$Pb($^8$He,$^7$He)$^{209}$Pb result was most affected, increasing by 100 mb to give a summed cross section approximately a factor of 1.4 times greater than the corresponding $^{208}$Pb($^6$He,$^5$He)$^{209}$Pb one, much closer to the ratio of the projectile overlap spectroscopic factors. It is impossible to say which value for the $^{208}$Pb($^8$He,$^7$He)$^{209}$Pb stripping cross section is most realistic; comparison with the inclusive $^6$He yield is inconclusive since $^6$He ejectiles may also result from $^{208}$Pb($^8$He,$^6$He)$^{210}$Pb transfer and breakup reactions and $^6$He$+n$ coincidence measurements are not possible with currently available $^8$He beam intensities. Empirical optical potentials for $^7$He and $^5$He projectiles are, of course, unavailable due to the unbound nature of these nuclei. Thus, the test calculations show that while the calculated stripping cross section for the $^8$He projectile is rather sensitive to the choice of exit channel optical potential—which cannot be fixed reliably with available data—the phenomenon under investigation, the influence of the coupling on the elastic scattering angular distributions, is much less so. This apparent lack of correlation between the magnitude of the stripping cross section and the influence of the stripping coupling on the elastic scattering is by no means unusual; it is often found that a large cross section is no guarantee that a particular reaction will have a large coupling effect on the elastic scattering and *vice versa*.

Before considering the DPPs, which were obtained by inversion of the elastic scattering $S$-matrix $S_L$ using the iterative-perturbative (IP) $S_L \rightarrow V(r)$ inversion method [11], we examine the coupling effect on $S_L$. It is important for such inversion to eliminate any small-amplitude numerical "noise" from $S_L$; such noise does not affect the observables, the angular distributions in this case, but can cause difficulties in the inversion process. After some experimentation it was found that calculations based on optical model potentials with somewhat deeper imaginary parts in the nuclear interior (i.e., with larger $W$ values) than those published in Ref. [1] eliminated almost all such noise from the $S$-matrix elements.
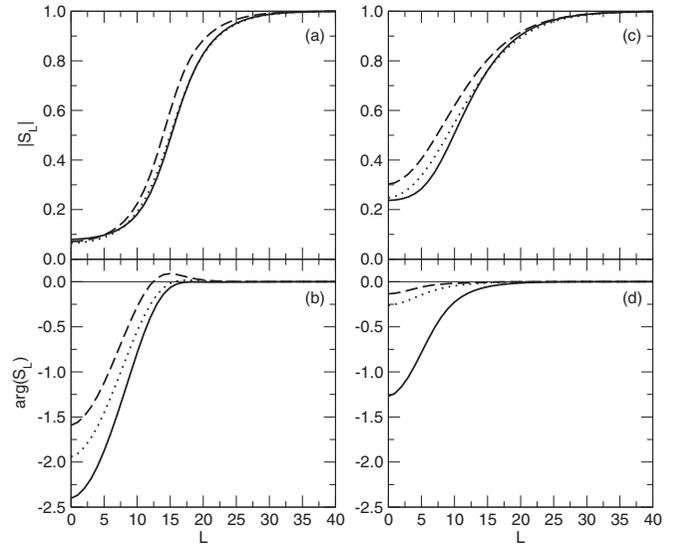


FIG. 2. (a) $|S_L|$ and (b) $\arg(S_L)$ for 22 MeV $^8$He $+^{208}$Pb. (c) $|S_L|$ and (d) $\arg(S_L)$ for 22 MeV $^6$He $+^{208}$Pb. The solid and dashed curves denote the full CRC and bare, no-coupling calculations, respectively. The dotted curves denote the corresponding quantities obtained from optical model fits with the parameters of Table I.

In Fig. 2 we show both $\arg(S_L)$ and $|S_L|$ for $^8$He and $^6$He for the bare, no-coupling calculations and the full CRC calculations. For comparison we also show the $S_L$ generated by optical model calculations using the parameters of Table I.

We see immediately that for both systems the most conspicuous coupling effect is on $\arg(S_L)$; although the effect on $|S_L|$ is by no means negligible that on $\arg(S_L)$ is large, particularly so for $^6$He $+^{208}$Pb. There are, however, significant differences in the coupling effect for the two systems. It is just visible on Fig. 2 (a) that $|S_L|$ for $^8$He $+^{208}$Pb exhibits a "wrong way" coupling effect [9] in that the $1n$-stripping coupling *increases* $|S_L|$ for low ($L < 5$) partial waves, whereas for $^6$He we see the more usual reduction of $|S_L|$ by the coupling for all $L$. The small increase in $|S_L|$ near $L = 0$ may be linked to the fact, which is not very clear in the linear plot of Fig. 1, that the angular distribution at 180° for $^8$He, while falling lower by an order of magnitude than for $^6$He, is actually slightly *increased* by the coupling. For $^8$He, $|S_L|$ is visibly reduced by the stripping coupling up to $L \approx 28$ whereas, for $^6$He, $|S_L|$ is almost unmodified beyond $L \approx 21$. The largest differences are, however, in the effect of coupling on $\arg(S_L)$. For $^8$He, the $1n$-stripping coupling eliminates the slight positive peak in $\arg(S_L)$ at $L \approx 12$ and in general has a large effect, making $\arg(S_L)$ more negative at all $L$. The coupling influence on $\arg(S_L)$ for $^6$He is much more important, acting to make $\arg(S_L)$ considerably more negative for most partial waves. We note that $|S_L|$ for the OM fits to the elastic scattering data agrees quite well with $|S_L|$ for the CRC calculations—the slightly worse agreement for $^6$He probably reflects the fact that the $^6$He $+^{208}$Pb CRC result is not quite as close to the optical model best fit as is the case for $^8$He—but the agreement for $\arg(S_L)$ is not so good. This is particularly striking for $^6$He where the optical model is much closer to

the no-coupling result than the full CRC one, despite the fact that the full CRC calculation gives an angular distribution much closer to the best-fit optical model one than the bare calculation. This suggests that for these systems where the imaginary potential appears to have the dominant influence on the elastic scattering angular distributions the observable—the angular distribution—is much less sensitive to $\arg(S_L)$ than to $|S_L|$. This is probably because in such systems there is no interference between near-side and far-side amplitudes. For light-ion scattering, nucleons in particular, changes in $\arg(S_L)$ correspond primarily to changes in the real potential and changes in $|S_L|$ correspond primarily to changes in the imaginary part. However, for strongly absorbed projectiles, the reverse can be the case (see Ref. [12]).

## III. THE DYNAMIC POLARIZATION POTENTIALS

In Fig. 3 we compare the DPPs induced by $1n$ stripping in the $^8$He $+^{208}$Pb and $^6$He $+^{208}$Pb systems as obtained by $S_L \to V(r)$ inversion. The DPPs are arrived at by subtracting the relevant bare optical model potentials from the potentials obtained by inverting the $S_L$ of the full CRC calculations. While it is immediately apparent that there are important similarities in the DPPs for the two systems it is also clear that there are significant differences. The similarities are largely qualitative; both systems exhibit significant attractive real and absorptive imaginary features, although the $^6$He DPP does have two large repulsive peaks flanking the region of attraction and a large emissive peak centered at about 9 fm that are not present in the $^8$He DPP. The somewhat undulatory ("wavy") nature of the DPPs is a general property of local and $L$-independent DPPs that exactly represent the contribution of coupled channels. It has been shown in Ref. [13] that
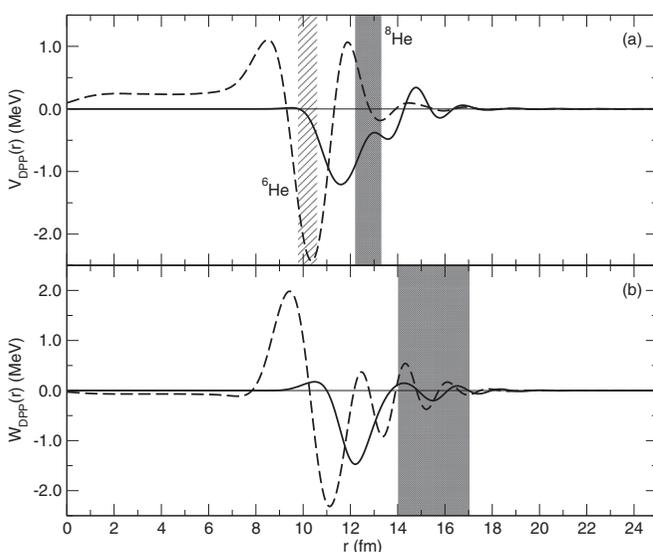
these undulations can be related to the angular momentum dependence of the formal DPP (see Ref. [14]).

The significant differences in the DPPs for the two systems are as follows: (i) the magnitudes of the main features of the $^6$He DPP are larger than those for $^8$He and (ii) the main attractive and absorptive features of the $^8$He DPP occur at significantly larger radii than do the corresponding features of the $^6$He DPP. For the absorption this displacement is approximately 1 fm while for the attraction it is perhaps somewhat less, although the wider, more structured nature of the attractive feature in $^8$He makes the comparison less precise for the real part of the DPP. All these structures are at radii smaller than the strong absorption radii as extracted from the CRC calculations, 13.5 fm for $^8$He $+^{208}$Pb and 12.5 fm for $^6$He $+^{208}$Pb, defined as the distance of closest approach of a classical Coulomb orbit for $L$ where $|S_L^{\mathrm{CRC}}| = 0.5$. The imaginary DPPs are also outside the radial region where the various Woods-Saxon form empirical optical model potentials obtained by alternative fits to the data for a given projectile coincide [1], denoted by the shaded area in Fig. 3(b). The most conspicuous features of the real DPPs, however, do fall within the regions where the corresponding real parts of these empirical optical model potentials cross, denoted by the hatched and shaded areas in Fig. 3(a) for $^6$He and $^8$He, respectively.

How, then, are the inverted potentials, and the resulting DPPs, to be interpreted? The following main features of the DPPs are well established by the inversion process: the absorptive structures centered at 11 and 12 fm in Fig. 3(b) and the attractive structures centered at 10.5 and 11.5 fm in Fig. 3(a). Clearly, if the DPPs were omitted, thus leaving the bare potential, the angular distributions would not fit the data. However, the real DPPs largely lie in radial ranges where the details of the potential are not strongly determined by the fit to the data. There are problems evaluating the imaginary DPPs that lie in the region where the angular distributions determine the parameters of a Woods-Saxon potential quite well. For that reason the oscillations in the imaginary DPPs in the shaded area of Fig. 3(b) are experimentally unverifiable. Moreover, we have seen that the elastic scattering angular distributions can be quite well fitted by CRC calculations where the parameters of the imaginary part of the Woods-Saxon potential alone are adjusted (see Table I). The DPP represented as the difference of the refitted and bare potentials therefore has a zero real component in this representation.

Thus, although the radial forms of the real and imaginary DPPs are well established by the inversion procedure, their specific forms appear to be inaccessible to experiment. It could therefore be argued that the details of the DPPs belong more to metaphysics than to physics, but this is not so for several reasons: (i) At higher energies, we expect that elastic scattering will be able to discern the radial shapes of the OMP for the same reactions, opening the possibility of a consistent picture of local DPPs over a range of energies and for different projectile-target combinations. (ii) The DPPs determined here are the local and $L$-independent equivalents of the formal DPPs. There is every possibility that this nonlocality will be important for barrier penetration, for example; it should be remembered that the OMP defined to fit elastic scattering may

FIG. 3. Real (a) and imaginary (b) parts of the DPP due to $1n$ stripping for 22 MeV $^8$He $+^{208}$Pb (solid curves) and $^6$He $+^{208}$Pb (dashed curves). See text for an explanation of the hatched and shaded areas.

not be the appropriate potential for other reactions. (iii) Related to this is the fact that the $S_L$-equivalent DPP is not identical to the wave-function-equivalent DPP; the implications of this are discussed by Hussein *et al.* [15], and the exact $S_L$-equivalent DPPs calculated here afford the opportunity to compare the effects of these alternative representations of the DPP. (iv) The generation of DPPs by inelastic and reaction processes is a universal feature of nucleus-nucleus scattering, a fact often neglected in the evaluation of folding models which are almost invariably based on a local density assumption. This motivates a general understanding of dynamic polarization contributions.

We remark that there do exist elastic scattering cases, such as certain instances of nucleon scattering, where precise data have revealed the inadequacy of folding models and pointed to explicit $L$ dependence that can be linked to reaction channel coupling. From this perspective, the present results have the possibility of becoming part of a more general understanding of nuclear interactions that goes beyond local folding models based on local density models. The present results also exemplify the inadequacy of the method, e.g., Ref. [16], of determining DPPs by subtracting bare potentials from the potentials refitted to scattering observables calculated with coupled channels methods.

## IV. SUMMARY AND DISCUSSION

New precise angular distribution data for the elastic scattering of $^8$He from a $^{208}$Pb target at the near-barrier laboratory energy of 22 MeV are different in significant ways from the existing $^6$He $+^{208}$Pb elastic scattering data at the same incident energy. In this work we have investigated, for both systems, the influence on the elastic scattering of coupling to single-neutron-stripping channels by means of CRC calculations. We have then compared, for $^6$He and $^8$He projectile nuclei, the local and $L$-independent representations of the DPPs generated by this coupling.

Many processes in addition to coupling to stripping channels contribute, beyond the lowest-order folding model, to the interaction between projectiles and target nuclei. A particular example is projectile breakup which is known to generate a very long absorptive tail in the case of $^6$He (see, e.g., Refs. [12,17]). However, because there is no simple model for the breakup of $^8$He, we have here limited our study to a comparison of the single-neutron-stripping coupling. We note that two-neutron stripping, i.e., the ($^6$He,$^4$He) and ($^8$He,$^6$He) reactions, is known to be an important contributor to the total reaction cross section for systems involving $^6$He [18–23] and $^8$He [24] projectiles incident on heavy targets. However, realistic calculation of this reaction is not possible due to the large positive $Q$ values that favor population of states in the $^{210}$Pb residual nucleus at excitation energies where there is little or no structure information available.

The single-neutron-stripping coupling has a significant effect on the elastic scattering angular distributions for both systems (see Fig. 1). However, there is a conspicuous qualitative difference between the two systems because the stripping coupling for $^8$He $+^{208}$Pb gives rise to a significant reduction of the elastic scattering cross section in the angular region where the Coulomb rainbow peak would normally

occur, whereas for $^6$He $+^{208}$Pb its influence is negligible in this region. This difference may be examined in more detail through a comparison of the DPPs, obtained in this work by inversion of the CRC $S_L$.

A conspicuous difference between the DPPs for the two systems is that the absorption generated by the $1n$-stripping coupling appears at a larger nuclear separation for $^8$He than for $^6$He. This is opposite to the case of the total absorption in these systems, as evidenced by the distance of closest approach where the elastic scattering first deviates significantly from the Rutherford value, which is much larger (19.5 fm) for $^6$He than it is for $^8$He (16.2 fm) [1]. Coupling to breakup is known to induce long-range absorption for $^6$He (see, e.g., Refs. [12,17]) and may be assumed to have a similar, though weaker, effect for $^8$He. It follows that the empirical optical model potential is dominated by the long-range breakup coupling effects in the region where it is well determined by the data, despite the influence demonstrated here of the single-neutron-stripping coupling on the elastic scattering angular distributions. It is for future work to determine whether this holds true at higher energies.

*All* elastic scattering is subject to dynamical processes that depend upon the specific nature of the interacting nuclei. These processes, of which the stripping coupling studied here is a single example, are not accounted for in folding models based on local density approximations. It is therefore desirable to establish systematic properties of the DPPs resulting from these processes. Moreover, because the formal DPPs are nonlocal and $L$ dependent (see, e.g., Ref. [14]) it is also desirable that the local equivalents be determined by an inversion procedure that fully captures these features in a local form. We note, for example, that the DPPs presented herein, which precisely reproduce the elastic channel $S_L$, exhibit certain undulatory features. Such features are, in fact, a general feature of DPPs, something that is not evident in DPPs calculated using the widely used weighted trivially equivalent local potential (TELP) procedure, for example, those in Ref. [15]. Explicit comparisons between exact $S$-matrix and weighted TELP inversions can be found in Refs. [25,26]. In specific cases the TELP and exact $S$-matrix inverted DPPs give similar results, leading to the same physical conclusions (see, e.g., Refs. [12,17] for the case of $^6$He breakup), although Refs. [25,26] show that one should be cautious about drawing conclusions from the details of TELP DPPs.

We have presented significant differences in the influence of coupling to single-neutron stripping on the elastic scattering angular distributions for the $^6$He and $^8$He $+^{208}$Pb systems at the near-barrier laboratory frame energy of 22 MeV. The coupling effect on the imaginary parts of the optical model potentials was found to scale well with the difference in spectroscopic factor for the two projectile-ejectile overlaps, unlike the calculated stripping cross sections. This provides a further instance of the influence of coupling to a particular reaction not being correlated with the cross section calculated for that reaction. The DPPs indicate that the absorption due to single-neutron stripping takes place at larger radii for $^8$He than for $^6$He, in contrast to the total absorption in these systems. An investigation of the variation with incident energy of the DPPs is left for future work.

[1] G. Marquínez-Durán *et al.*, Phys. Rev. C **94**, 064618 (2016).
[2] I. J. Thompson, Comput. Phys. Rep. **7**, 167 (1988).
[3] D. G. Kovar, N. Stein, and C. K. Bockelman, Nucl. Phys. A **231**, 266 (1974).
[4] N. Keeley *et al.*, Phys. Lett. B **646**, 222 (2007).
[5] N. Keeley and N. Alamanos, Phys. Rev. C **77**, 054602 (2008).
[6] Ł. Standyło *et al.*, Phys. Rev. C **87**, 064603 (2013).
[7] R. S. Mackintosh and N. Keeley, Phys. Rev. C **85**, 064603 (2012).
[8] R. S. Mackintosh and N. Keeley, Phys. Rev. C **90**, 044601 (2014).
[9] R. S. Mackintosh, Phys. Rev. C **88**, 054603 (2013).
[10] J. Cook, Nucl. Phys. A **388**, 153 (1982).
[11] V. I. Kukulin and R. S. Mackintosh, J. Phys. G **30**, R1 (2004).
[12] R. S. Mackintosh and N. Keeley, Phys. Rev. C **79**, 014611 (2009).
[13] R. S. Mackintosh, Phys. Rev. C **94**, 034602 (2016).
[14] G. H. Rawitscher, Nucl. Phys. A **475**, 519 (1987).
[15] M. S. Hussein, M. P Pato, L. F. Canto, and R. Donangelo, Phys. Rev. C **23**, 926 (1981).
[16] R. S. Mackintosh, Nucl. Phys. A **164**, 398 (1971).
[17] J. P. Fernández-García, M. Rodríguez-Gallardo, M. A. G. Alvarez, and A. M. Moro, Nucl. Phys. A **840**, 19 (2010).
[18] D. Escrig *et al.*, Nucl. Phys. A **792**, 2 (2007).
[19] L. Acosta *et al.*, Phys. Rev. C **84**, 044604 (2011).
[20] J. P. Fernández-García, M. A. G. Alvarez, A. M. Moro, and M. Rodríguez-Gallardo, Phys. Lett. B **693**, 310 (2010).
[21] J. P. Bychowski *et al.*, Phys. Lett. B **596**, 26 (2004).
[22] P. A. DeYoung *et al.*, Phys. Rev. C **71**, 051601 (2005).
[23] J. J. Kolata, H. Amro, F. D. Becchetti, J. A. Brown, P. A. DeYoung, M. Hencheck, J. D. Hinnefeld, G. F. Peaslee, A. L. Fritsch, C. Hall, U. Khadka, P. J. Mears, P. O'Rourke, D. Padilla, J. Rieth, T. Spencer, and T. Williams, Phys. Rev. C **75**, 031302 (2007).
[24] A. Lemasson *et al.*, Phys. Lett. B **697**, 454 (2011).
[25] D. Y. Pang and R. S. Mackintosh, Phys. Rev. C **84**, 064611 (2011).
[26] R. S. Mackintosh and N. Keeley, arXiv:1610.07378.